Neuron, Vol. 32, 775–786, December 6, 2001, Copyright ©2001 by Cell Press

A Photoreceptor-Specific Cadherin Is Essential for the Structural Integrity of the Outer Segment and for Photoreceptor Survival

Amir Rattner,[1] Philip M. Smallwood,[1,3] John Williams,[1,3] Carol Cooke,[4] Andrey Savchenko,[5] Arkady Lyubarsky,[5] Edward N. Pugh, Jr.,[5] and Jeremy Nathans[1,2,3,6]
[1]Department of Molecular Biology and Genetics
[2]Department of Neuroscience
Department of Ophthalmology
[3]Howard Hughes Medical Institute
[4]Microscope Facility
Johns Hopkins University School of Medicine
Baltimore, Maryland 21205
[5]Department of Ophthalmology
University of Pennsylvania School of Medicine
Philadelphia, Pennsylvania 19104

Summary

A cadherin family member, prCAD, was identified in retina cDNA by subtractive hybridization and high throughput sequencing. *prCAD* is expressed only in retinal photoreceptors, and the prCAD protein is localized to the base of the outer segment of both rods and cones. In *prCAD*$^{-/-}$ mice, outer segments are disorganized and fragmented, and there is progressive death of photoreceptor cells. *prCAD* is unlikely to be involved in protein trafficking between inner and outer segments, since phototransduction proteins appear to be correctly localized and the light responses of both rods and cones are only modestly compromised in *prCAD*$^{-/-}$ mice. These experiments imply a highly specialized cell biological function for prCAD and suggest that localized adhesion activity is essential for outer segment integrity.

Introduction

Rods and cones are highly polarized sensory neurons that initiate the light response in the vertebrate retina. To efficiently capture light, vertebrate photoreceptors have evolved a greatly enlarged derivative of a nonmotile cilium referred to as the outer segment. The outer segment contains large quantities of the phototransduction proteins organized within a series of stacked membrane disks. Outer segments are renewed throughout life by the assembly of new disks at the base and by the shedding of older disks from the tip. Outer segment proteins are synthesized within the inner segment of the photoreceptor and are transported to the outer segment via the thin connecting cilium.

A number of inherited retinal degenerations are caused by mutations that disrupt the integrity or assembly of the outer segment. Alterations in peripherin/rds or ROM-1 (structural proteins within the outer segment disks) produce defects in disk morphogenesis (Sanyal et al., 1980; Travis et al., 1992; Clarke et al., 2000); mutations that alter rhodopsin's C terminus lead to accumulation of opsin within the cell body and in some cases an accumulation of vesicles at the outer segment base (Sung et al., 1994; Li et al., 1996); and mutations in three proteins that localize to the connecting cilium—myosin VIIa (Liu et al., 1999), KIF3A (Marszalek et al., 2000), and RPGR (Hong et al., 2000)—lead to accumulation of phototransduction proteins in the connecting cilium and/or the cell body, suggestive of a defect in vectorial protein transport from the inner to the outer segment. Each of these defects leads ultimately to photoreceptor cell death.

The cadherins are a large family of cell surface proteins defined by the presence of a variable number of extracellular cadherin domains (Yagi and Takeichi, 2000). Initially identified as the principal proteins responsible for calcium-dependent, homotypic cell-cell adhesion, cadherins are important for the development and function of many epithelial tissues (Tepass et al., 2000; Angst et al., 2001). Some members of the cadherin superfamily have been been found to interact with cell surface or extracellular matrix proteins: E-cadherin can interact with alphaE-β7 integrin (Cepek et al., 1994), and the protocadherin CNR1 binds to Reelin (Senzaki et al., 1999). The cytosolic domains of classical and desmosomal cadherins interact with catenins and plakophilin/desmoplakin, respectively, thereby anchoring and modulating the actin and intermediate filament cytoskeletons (Angst et al., 2001). Recently, it has been reported that the cytosolic domain of the CNR subfamily of cadherins can interact with the src-family tyrosine kinase fyn (Kohmura et al., 1998), suggesting a role for cadherins in signal transduction.

In the present work, we report the identification of a member of the cadherin superfamily, photoreceptor cadherin (prCAD), using subtraction and normalization of retina cDNA, high throughput sequencing, and database homology searches. prCAD is localized to the base of the outer segment at the junction between the photoreceptor inner and outer segments. Targeted disruption of the *prCAD* gene in the mouse results in disorganization of photoreceptor outer segments and a progressive loss in photoreceptor cells, indicating that prCAD is essential for outer segment architecture and photoreceptor survival.

Results

Identification and Primary Structure of prCAD

To identify genes expressed specifically in the retina, we constructed a bovine retina cDNA library that had been subtracted with bovine brain cDNA and normalized, as described previously (Rattner et al., 2000). An initial screen of 1000 partial cDNA sequences revealed a sequence with cadherin domains. As described below, this cadherin is expressed only in retinal photoreceptors and was therefore named photoreceptor cadherin (prCAD).

prCAD cDNA clones isolated from mouse, bovine, and chicken retina cDNA libraries code for proteins of 859, 867, and 865 amino acids, respectively, with 84% iden-

[6]Correspondence: jnathans@jhmi.edu

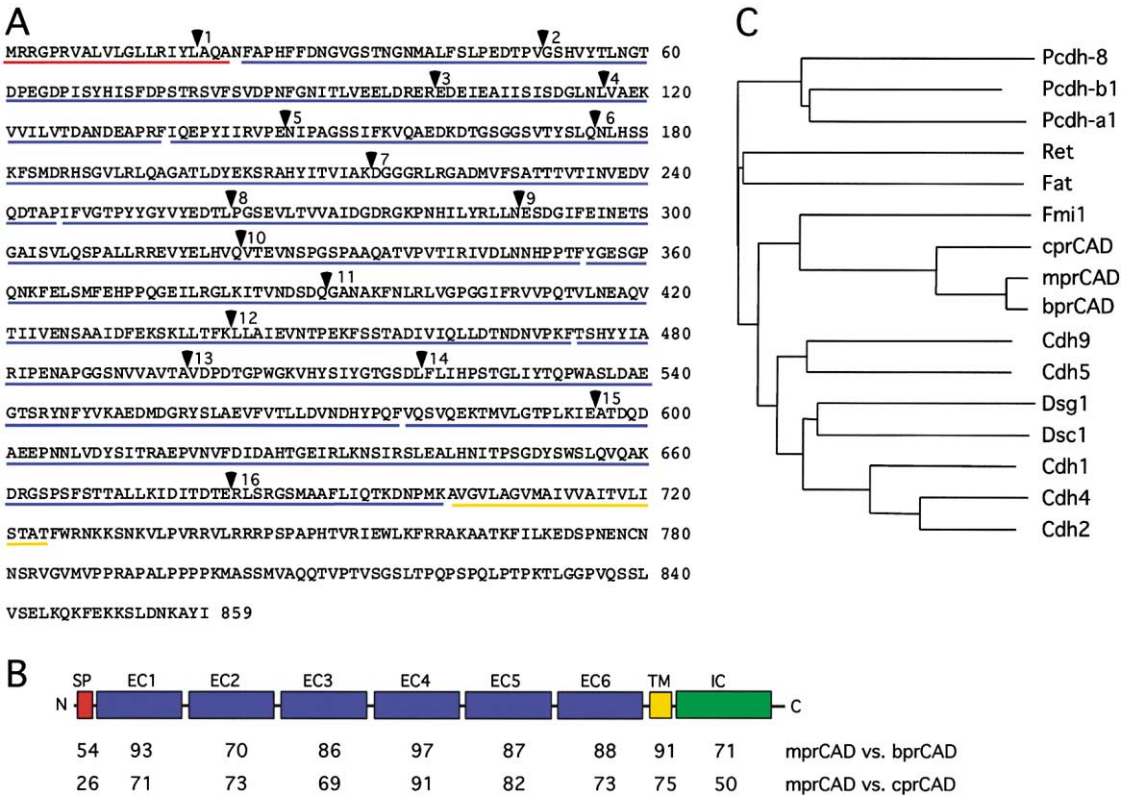

Figure 1. prCAD Protein Sequences

(A) Amino acid sequence of mouse prCAD. Intron positions are shown as numbered vertical arrowheads.

(B) Domain structure and percent amino acid identity between individual domains of bovine, mouse, and chicken prCADs. Abbreviations are as follows: SP, signal peptide; EC, extracellular domain; TM, transmembrane domain; and IC, intracellular domain.

(C) Sequence similarity between the amino terminal cadherin domain of prCAD and of representative members of the cadherin superfamily. By BLAST search of the GenBank database, no cadherin repeat shows higher homology to prCAD than those chosen for the dendrogram. Abbreviations are as follows: c, chicken; m, murine; and b, bovine; Cdh1, E-cadherin (GenBank accession number Z13009); Cdh2, N-cadherin (S42303); Cdh4, R-cadherin (L34059); Cdh5, VE-cadherin (X79981); Cdh9, T1-cadherin (AB035302); Dsg1, Desmoglien-1 (X56654); Dsc1, Desmocollin-1 (Z34522); Fat, Fat (X87241); Fmi1, Flamingo1 (AB028499); Pcdh-a1, Protocadherin-α1 (CNR, AF152305); Pcdh-b1, Protocadherin-β1 (AF152488); Pcdh-8, Protocadherin-8 (Arcadlin, AF061573); and Ret (X12949+X15262).

tity between the mouse and bovine prCADs and ~72% average identity between chicken prCAD and either of the mammalian prCADs (Figures 1A and 1B). A search of the high throughput human genome sequence in the GenBank database identified a single gene with high homology to bovine prCAD (>85% amino acid identity) that maps to chromosome 10. Localization of human *prCAD* to chromosome 10q22 (locus SHGC-11466) was confirmed using the TNG4 radiation hybrid panel.

The deduced prCAD amino acid sequences reveal a signal peptide, six extracellular cadherin repeats, a putative transmembrane domain, and a ~150 amino acid long cytoplasmic domain (Figures 1A and 1B). Although the overall arrangement and number of domains within prCAD conform to the structure of the protocadherins from the CNR subfamily of neuronal receptors, sequence alignment reveals that prCAD is not highly related to this subfamily. prCAD also shows only weak homology to invertebrate cadherins, which generally diverge significantly from vertebrate cadherins in extracellular repeat number and composition (Yagi and Takeichi, 2000). Since variability in the number and sequence of the extracellular cadherin repeats complicates comparisons among distantly related cadherins, Figure 1C simply shows a dendrogram based on comparisons of the most N-terminal domain from representative family member (Nollet et al., 2000). This comparison shows that prCAD is not highly related to any of the major subfamilies of cadherins and thus defines a new branch in the cadherin tree. The cytoplasmic domain of prCAD shows no significant homology to any other sequences in the protein or translated DNA sequence databases. Several sequence blocks within this domain that show high interspecies conservation may represent protein interaction domains.

Tissue Distribution and Subcellular Localization of prCAD

Hybridization of a mouse *prCAD* cDNA probe to total RNA from various rat tissues revealed a 4.5 kb transcript present exclusively in the retina (Figure 2A). Similar results were obtained upon hybridization of a bovine *prCAD* probe to total RNA from bovine tissues (data not shown). The distribution of *prCAD* mRNA was further defined by in situ hybridization to mouse retina (Figure 2B) and bovine retina (data not shown). In both species,

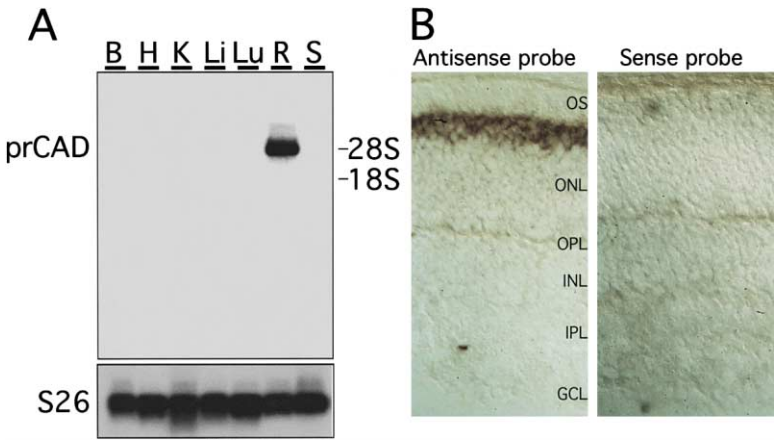

Figure 2. Distribution of *prCAD* Transcripts in Rodent Tissues

(A) RNA blot hybridization. The gel was loaded with 20 μg of total RNA from rat brain (B), heart (H), kidney (K), liver (Li), lung (Lu), retina (R), and spleen (S), and the filter was hybridized with radiolabeled probes from mouse *prCAD* (upper) or ribosomal protein S26 (lower). The mobilities of the 18S and 28S ribosomal RNAs are indicated.

(B) In situ hybridization to mouse retina localizes *prCAD* transcripts to photoreceptors. Mouse *prCAD* antisense probe (left) and sense probe (right). Abbreviations are as follows: OS, outer segments; ONL, outer nuclear layer; OPL, outer plexiform layer; INL, inner nuclar layer; IPL, inner plexiform layer; and GCL, ganglion cell layer.

prCAD transcripts were detected only in the outer nuclear layer, indicating expression in photoreceptors.

To localize the prCAD protein within photoreceptor cells, rabbit polyclonal antibodies were raised against the C-terminal 16 amino acids of mouse prCAD and against a fusion protein encompassing the first two cadherin domains. At the light microscope level, the two sets of antibodies produce identical patterns of immunostaining; the figures below present results obtained with the antipeptide antibodies. The specificity of the anti-prCAD antibodies was also verified by staining retinas from *prCAD*$^{+/-}$ and *prCAD*$^{-/-}$ mice, as discussed below. Labeling mouse retina sections with affinity-purified anti-prCAD antibodies shows that prCAD is present in rod photoreceptors and is localized to the junction between the photoreceptor inner and outer segments. This subcellular localization can be clearly demonstrated by double-labeling mouse retina sections with anti-prCAD antibodies in combination with monoclonal antibodies to either the Na/K ATPase, which is an inner segment protein (Figures 3A and 3C), or the cGMP gated channel (CNCG), which is an outer segment protein (Figures 3B and 3D). prCAD is also present at the inner segment/outer segment junction in cone photoreceptors as determined by double-labeling mouse retina sections with anti-prCAD antibody and peanut agglutinin, which specifically labels the extracellular matrix that ensheaths cones (Figures 3E and 3F). When viewed by confocal microscopy in a plane close to that of the retina, the prCAD signal appears crescent- or ring-shaped with a diameter of ~1.5 μm (Figure 3F), suggesting that most of the prCAD resides in or close to the lateral edge of the photoreceptor rather then in the much smaller connecting cilium.

Preembedding immunoelectron microscopy using affinity-purified anti-prCAD C-terminal antibodies and silver-enhanced immunogold labeling confirms the distribution observed by light microscopy and further localizes mouse prCAD to the base of the outer segment (Figure 4). Immunogold labeling was most prominent on the edges of nascent evaginating discs (Steinberg et al., 1980) on the side of the outer segment opposite the connecting cilium (Figures 4B and 4C). Control samples incubated either without primary rabbit antibodies or with a ~10-fold greater quantity of unrelated rabbit antibodies show no accumulation of immunogold at this site. Although these experiments cannot rule out the possibility that a population of antigenically masked prCAD proteins is present at the distal tip of the inner segment, the simplest interpretation of the data is that prCAD is localized to the base of the outer segment. No other protein with this subcellular distribution has thus far been described.

Photoreceptor Cell Death in *prCAD*$^{-/-}$ Mice

To study the in vivo function of prCAD, we generated a presumptive null mutation in the mouse germline by replacing exons 10–17 of the *prCAD* gene (which code for the C-terminal two-thirds of the protein) with the *PGKneo* selectable marker (Figures 5A and 5B). *prCAD* transcripts and prCAD protein are undetectable in the retinas of *prCAD*$^{-/-}$ mice, as shown by RNA blot hybridization (Figure 5C) and immunostaining of retina sections with antibodies directed against the C terminus (Figure 5D) or against the first two cadherin domains (data not shown). In the ERG and histologic analyses described below, no differences were observed between *prCAD*$^{-/-}$ mice maintained on 129 inbred or 129 X C57BL/6j backgrounds.

prCAD$^{-/-}$ mice are viable and fertile and show no overt anatomic or behavioral abnormalities, consistent with the tissue specificity of *prCAD* expression. In *prCAD*$^{-/-}$ mice, the development of the retina appears essentially normal as judged by its appearance at 1 month of age (Figure 6A). However, a progressive loss of photoreceptor cells is observed over the ensuing 5 months, with a 50% reduction in the number of nuclei in the outer nuclear layer by 6 months of age, the latest time point analyzed (Figures 6A and 6B). This cell loss appears to occur via apoptosis, as seen in a variety of mouse models of retinal disease (Chang et al., 1993; Lolley et al., 1994; Portera-Cailliau et al., 1994). In situ labeling of fragmented nuclear DNA using the TUNEL method revealed a significant increase in TUNEL-positive cells in the outer nuclear layer of *prCAD*$^{-/-}$ mice compared to their *prCAD*$^{+/-}$ littermates (Figures 6C and 6D). Photoreceptor cell death was detected in *prCAD*$^{-/-}$ retinas as early as 1 month of age (the earliest time tested), shortly after completion of retinal development. Although the total number of TUNEL-positive cells declines progressively with age, more TUNEL-positive photoreceptor cells were detected in *prCAD*$^{-/-}$ mice compared to their

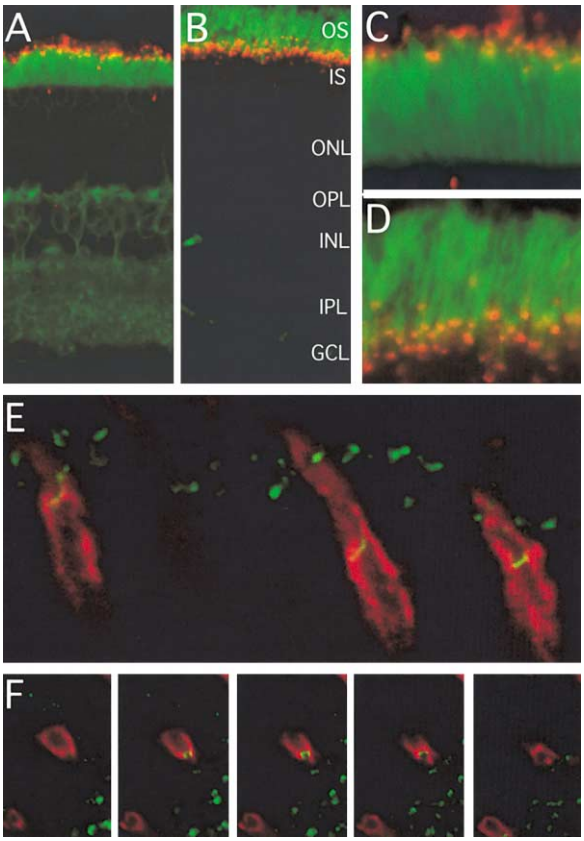

Figure 3. Immunolocalization of prCAD to the Junction between the Inner and Outer Segments of Rod and Cone Photoreceptors

Confocal images of prCAD in mouse retina visualized with affinity-purified rabbit anti-mouse prCAD antibodies and Texas red (A–D) or fluorescein (E and F) conjugated secondary antibody.

(A and C) Photoreceptor inner segments simultaneously visualized with mouse anti-Na/K ATPase antibody and fluorescein-conjugated secondary antibody.

(B and D) Photoreceptor outer segments simultaneously visualized with mouse anti-CNGC antibody and fluorescein-conjugated secondary antibody.

(C) and (D) show the inner segment-outer segment regions of (A) and (B), respectively, at higher magnification.

(E and F) Cone matrix sheaths simultaneously visualized with rhodamine-conjugated peanut agglutinin.

(E) Vertical section of mouse retina.

(F) A series of 0.5-μm-thick optical sections oriented close to the plane of the retina at the level of the connecting cilium. PrCAD immunoreactivity is confined to a small zone within the cone sheath at the level of the inner segment-outer segment junction.

prCAD$^{+/-}$ littermates at every age up to 6 months (the latest time point tested). Additionally, we observed activation of Muller glia in the *prCAD*$^{-/-}$ retina, as indicated by increased production of glial fibrillary acidic protein (GFAP; Figure 6E), a response that is seen in a variety of other photoreceptor degenerations (Semple-Rowland, 1991; de Raad et al., 1996; Hong et al., 2000).

Outer Segment Structure in *prCAD*$^{-/-}$ Mice

As noted in the introduction, the connecting cilium and its associated proteins at the inner segment-outer segment junction play an important role in vectorial transport of outer segment components. Mutations in some connecting cilium proteins such as myosin VIIa and RPGR, as well as in the putative transcription factor TULP1 (Hagstrom et al., 1999), result in the mislocalization of opsins and other outer segment proteins, changes that precede and may be the cause of photoreceptor cell death. To test whether outer segment protein transport is compromised in the absence of prCAD, 1-month-old *prCAD*$^{+/-}$ and *prCAD*$^{-/-}$ retinas were immunostained with antibodies to rhodopsin, S-cone opsin, ROM-1, and CNGC (Figures 7A–7H). No significant difference in the localization of any of these outer segment proteins was observed. Thus, photoreceptor cell loss in *prCAD*$^{-/-}$ mice is not likely to be the result of aberrant transport of the major protein components of the outer segment.

Close examination of the outer segment region of *prCAD*$^{+/-}$ and *prCAD*$^{-/-}$ retinas at the light microscope level (Figures 6A and 7A–7H) suggests that the *prCAD*$^{-/-}$ outer segments are shorter and disorganized. This impression was confirmed by transmission electron microscopy, which showed that the *prCAD*$^{-/-}$ outer segments were shorter, misaligned, and composed of large swirls of membranes with many imperfectly stacked disks (Figures 7J and 7K). In contrast, *prCAD*$^{+/-}$ outer segments are well aligned and appear to be indistinguishable from those of wild-type mice (Figure 7I). Consistent with the thinner outer segment layer in *prCAD*$^{-/-}$ retinas, immunoblot analysis of partially purified outer segments, prepared by gently shaking isolated retinas from 1-month-old littermates, revealed an approximately 2-fold decrease in rhodopsin and arrestin content in outer segments from *prCAD*$^{-/-}$ retinas compared to those from *prCAD*$^{+/+}$ retinas (data not shown). Microscopic examination of these mechanically isolated outer segments revealed predominantly small fragments from *prCAD*$^{-/-}$ retinas compared to largely intact outer segments from *prCAD*$^{+/+}$ retinas (data not shown). By contrast, the inner segments and RPE appear to be largely or completely unaffected in *prCAD*$^{-/-}$ mice. Thus, photoreceptor degeneration in the *prCAD*$^{-/-}$ mouse retina is preceded by abnormal morphogenesis and/or stability of the photoreceptor outer segment.

Analysis of Retinal Function of prCAD$^{-/-}$ Mice

We used electroretinography to assess retinal function, measuring scotopic b-waves, a-waves, and cone-driven b-waves. The scotopic b-wave response is a field potential thought to be generated principally by rod bipolar cells, each of which amplifies the dim-flash responses of about 20 rods (reviewed in Pugh et al., 1998). Figures 8A–8C show ERGs of dark-adapted *prCAD*$^{+/+}$, *prCAD*$^{+/-}$, and *prCAD*$^{-/-}$ mice in response to very dim flashes. From such scotopic b-wave response families, we extracted three descriptive parameters: the saturating amplitude ($b_{max,scot}$), the half-saturating intensity ($I_{0.5}$), and the time to peak(t_{peak}). Estimations of $b_{max,scot}$ and $I_{0.5}$ were estimated from hyperbolic saturation functions of the form $b_{peak}/b_{max} = I/(I + I_{0.5})$, fitted to the peak amplitude versus intensity plots of the b-wave data with a nonlinear least-squares method. The best-fitting parameters for the mice of Figure 8 were (b_{max}, $I_{0.5}$) = (275 μV, 3×10^{-4} cd s m^{-2}) for the *prCAD*$^{+/+}$, (400 μV, 8×10^{-4} cd s m^{-2}) for the *prCAD*$^{+/-}$, and (290 μV, 1.1×10^{-4} cd s m^{-2}) for the *prCAD*$^{-/-}$, while t_{peak} was obtained directly from the

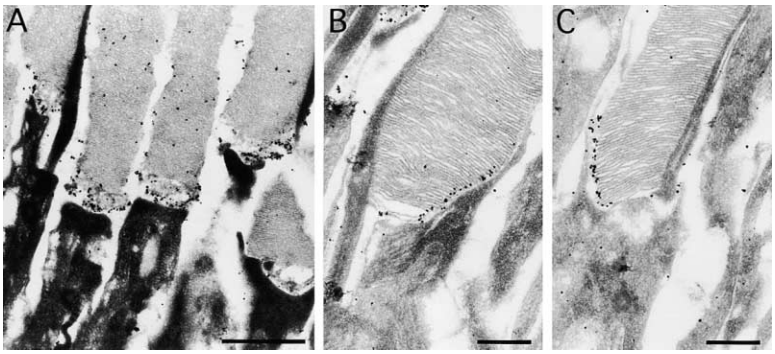

Figure 4. prCAD Localizes to the Base of Outer Segment

Preembedding immunolabeling of mouse retina using silver-enhanced immunogold and anti-prCAD C-terminal antibodies. The immunogold label localizes to the most superficial regions of the evaginating discs at the base of the outer segment. The bar in (A) equals 1 μm; the bars in (B) and (C) are 0.5 μm.

responses to the two least-intense flashes in the series (symbols superimposed on traces). Table 1 summarizes the results of applying the same protocol and analysis to 13 mice of the three *prCAD* genotypes.

The a-wave of the murine ERG arises almost exclusively from the suppression of rod circulating current (cf., Pugh et al., 1998), and so, to characterize rod photoreceptor function, we recorded and analyzed a-waves of each animal. Figures 8D–8F show records of the same mice whose b-waves are shown in Figures 8A–8C. In Figure 8G–8I, the a-waves have been normalized to their saturating amplitudes (a_{max}) and fitted with equation 1 to extract a parameter, *KA*, characterizing the amplification of the rod transduction cascade (see Experimental Procedures).

The photopic or cone-driven ERG b-wave is thought to originate in cone ON-bipolar cells. Cone b-waves were also recorded from each mouse (data not shown) by measuring responses in the presence of a rod-saturating background, as described in Lyubarsky et al. (1999). Summary parameters, including the saturating amplitude ($b_{max,phot}$) and the relative sensitivity of the b-wave near the spectral sensitivity peaks of the two cone pigments (S_{UV}/S_M) are given in Table 1.

Several response parameters that reflect the saturating current densities of key retinal cell types ($b_{max,scot}$, a_{max}, $b_{max,phot}$) are consistently larger for the sample of $prCAD^{+/-}$ mice than they are for the sample of $prCAD^{+/+}$ mice. This is likely to be an effect of the small sample size and could possibly reflect differences between litters from which the animals were drawn. On the assumption that there is no functional enhancement effect of *prCAD* heterozygosity, we pooled the $prCAD^{+/-}$ and $prCAD^{+/+}$ samples for statistical analysis of the effect of *prCAD* deletion. Only two highly reliable effects were found: (1) a_{max}, the saturating a-wave amplitude, is diminished by 2- to 3-fold in the $prCAD^{-/-}$ relative to $prCAD^{+/+}$ and $prCAD^{+/-}$ mice; and (2) $b_{max,phot}$, the saturating amplitude of the cone-driven b-wave response, is diminished about 2-fold in $prCAD^{-/-}$ mice. Both these effects were significant at the $p = 0.0005$ level (one-tailed t test, 11 df). Both effects remain highly significant if the $prCAD^{-/-}$ sample is tested against either the $prCAD^{+/-}$ or $prCAD^{+/+}$ samples, as opposed to the pooled sample.

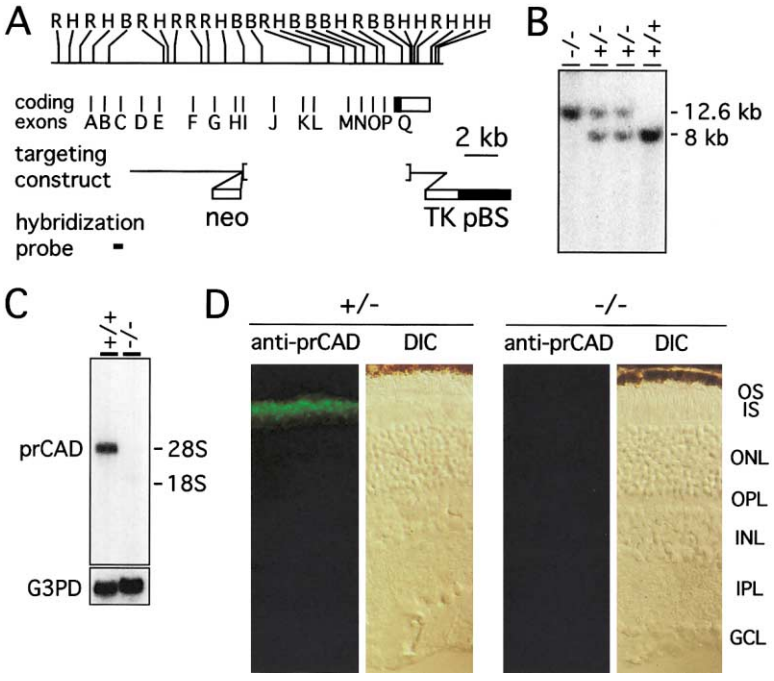

Figure 5. Targeted Mutation of the *prCAD* Locus

(A) *PrCAD* genomic locus (top) and targeting construct (bottom). The locations of coding exons A–Q are shown underneath a restriction map. Abbreviations are as follows: B, *Bam*H I; E, *Eco*R I; and H, *Hind* III. Homologous recombination replaces *prCAD* exons J–Q, coding for the C-terminal 571 amino acids, with the *PGK-neo* selectable marker.

(B) Blot of *Bam*H I digested genomic DNA from $prCAD^{-/-}$, $prCAD^{+/-}$, and $prCAD^{+/+}$ mice using the 5′ flanking hybridization probe indicated in (A).

(C) Blot of total retina RNA from $prCAD^{+/+}$ and $prCAD^{-/-}$ mice. The filter was hybridized with cDNA probes from mouse prCAD (upper) or glucose-3-phosphate dehydrogenase (G3PD; lower). The mobilities of the 18S and 28S ribosomal RNAs are indicated.

(D) Retinas of $prCAD^{+/-}$ (left) and $prCAD^{-/-}$ (right) sibling mice immunostained with anti-prCAD antibodies and fluorescein-conjugated secondary antibody. Within each pair of panels, the fluorescent image is shown on the left, and the differential interference contrast (DIC) image is shown on the right.

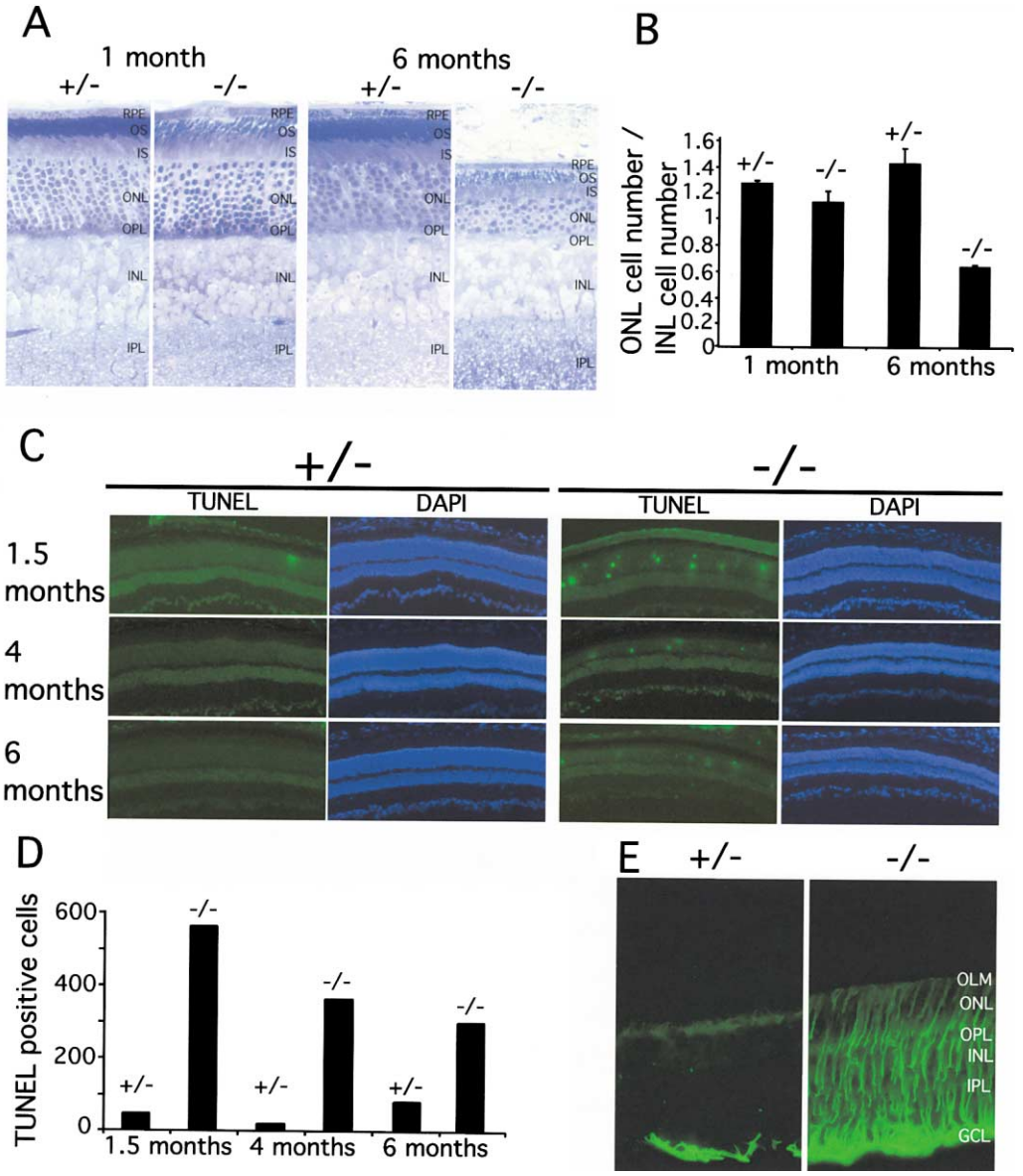

Figure 6. Progressive Degeneration of Photoreceptors in *prCAD*$^{-/-}$ Retinas

(A) 0.5 μm plastic sections of retinas from *prCAD*$^{+/-}$ and *prCAD*$^{-/-}$ mice at 1 and 6 months of age stained with toluidine blue. In *prCAD*$^{-/-}$ retinas at both ages, the outer segments appear disorganized, and in *prCAD*$^{-/-}$ retinas at 6 months, there is a marked reduction in the thickness of the ONL.

(B) Histogram showing the ratio of ONL to INL nuclei in *prCAD*$^{+/-}$ and *prCAD*$^{-/-}$ retinas at 1 and 6 months. The histogram shows an average of three sections; the bars show standard deviation.

(C) TUNEL-positive cells visualized by incorporation of fluorescein-conjugated dUTP (left three panels in each set) and cell nuclei visualized with DAPI (right three panels in each set) in *prCAD*$^{+/-}$ (left) and *prCAD*$^{-/-}$ (right) retinas at the ages indicated on the left.

(D) Histogram showing the total number of TUNEL-positive cells in *prCAD*$^{+/-}$ and *prCAD*$^{-/-}$ retinas at the indicated ages. Each bar represents the total number of TUNEL-positive cells from twelve 14-μm-thick sections that uniformly sample the retina.

(E) GFAP is induced in retinal Muller glia in *prCAD*$^{-/-}$ retinas. *prCAD*$^{+/-}$ (left) and *prCAD*$^{-/-}$ (right) retinas were stained with polyclonal anti-GFAP antibodies and fluorescein-conjugated secondary antibody. The abbreviation OLM refers to outer limiting membrane.

Discussion

Identification and Characterization of prCAD

This work describes the discovery of prCAD, a photoreceptor-specific member of the cadherin superfamily. The highly localized expression of *prCAD* is in contrast to the widespread expression reported for other cadherin family members. Although a number of other cadherins are expressed in the retina, each is also expressed in many nonretinal cells, and none have thus far been localized exclusively to photoreceptors (Wohrn et al., 1998; Honjo et al., 2000). Within the photoreceptor cell, prCAD is confined to the base of the outer segment. While several proteins (including myosin VIIa, RPGR, RPGR-interacting protein [RPGRIP], KIF3A, and γ-tubulin) have been localized to the connecting cilium between

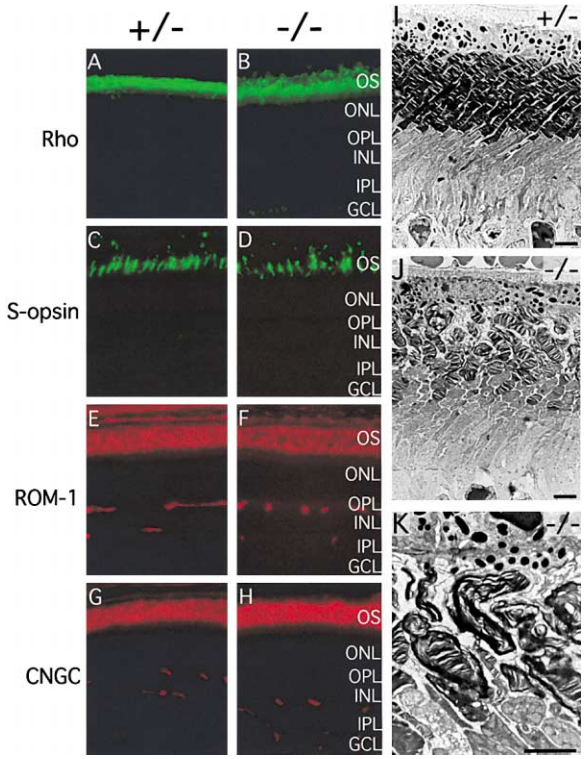

Figure 7. Structure of *prCAD*$^{-/-}$ Outer Segments

(A–H) Normal localization of outer segment proteins in *prCAD*$^{-/-}$ retinas. Immunohistochemistry on 1-month-old *prCAD*$^{+/-}$ (A, C, E, and G) or *prCAD*$^{-/-}$ (B, D, F, and H) retinas with antibodies to the four outer segment proteins indicated on the left. In (E–H), the fluorescent signal in the inner retina arises from the binding of the secondary anti-mouse antibody to IgG in retinal blood vessels.

(I–K) Disorganization of *prCAD*$^{-/-}$ outer segments. Electron micrographs of the inner segment, outer segment, and RPE region in 1-month-old *prCAD*$^{+/-}$ (I) and *prCAD*$^{-/-}$ (J and K) retinas. Outer segments in the *prCAD*$^{-/-}$ retina are fragmented and disorganized. The bars in (I) and (J) are 2 μm; the bar in (K) is 1 μm.

inner and outer segments (Muresan et al., 1993, 1997; Beech et al., 1996; Liu et al., 1997; Whitehead et al., 1999; Hong et al., 2000, 2001) and the ankle-link antigen (an as-yet-undefined antigen shared by auditory hair cells and photoreceptors) has been localized to the distal plasma membrane of the inner segment and its associated calycal processes in the chicken retina (Goodyear and Richardson, 1999), to date no proteins have been reported with the same localization as prCAD. Unlike the integral membrane proteins of the outer segment that have been previously studied, prCAD is not present to any appreciable extent in either the disc membrane or the outer segment plasma membrane distal to the most basal region of the outer segment. It will therefore be of significant interest to determine the mechanism by which prCAD remains localized at the base of the outer segment while being effectively excluded from the other, far more abundant, outer segment membranes that originate from it.

Outer Segment Structure and prCAD

Outer segment renewal constitutes the major biosynthetic activity of photoreceptor cells. In mammals, several microns of outer segment, containing roughly 80–90 disks, are assembled from the connecting cilium per day (Young, 1971). At present, the molecular components and processes involved in orchestrating the uniform growth of outer segments, the formation and stacking of outer segment disks, the precise parallel alignment of outer segments, and the adhesion between outer segments and the RPE remain largely unknown. As described below, the localization of prCAD and the phenotype of *prCAD*$^{-/-}$ mice suggests that prCAD may play a role in some or all of these processes.

Early work on cadherin function focused on the role of cadherins in cell-cell adhesion. Such a role seems unlikely for prCAD. The proximal outer segment where prCAD is localized is several microns distal to the outer limiting membrane, the boundary formed by tight junctions at the base of the photoreceptor inner segments. The outer limiting membrane also marks the terminal extent of the Muller glia. At the level of the inner segment-outer segment junction, ultrastructural analyses show no evidence of intimate cell-cell contact; at this level each photoreceptor appears to be surrounded only by an annulus of extracellular matrix.

These considerations suggest models in which the extracellular domain of prCAD interacts either with extracellular matrix molecules or with membrane proteins in the same cell. In the former case, prCAD could interact with interphotoreceptor matrix molecules, potentially organizing the sheath of ECM molecules that surrounds each outer segment or contributing to photoreceptor-RPE adhesion by anchoring the point of attachment of these two cell types to the proximal outer segment. In the latter case, prCAD-mediated adhesion might maintain inner segment-outer segment proximity or participate in the orderly folding of outer segment plasma membranes to form the internal disks. In particular, the localization of prCAD to the edges of the nascent evaginating discs suggests that prCAD could play a role in disc growth or the simultaneous "zippering up" of the rim between adjacent pairs of nascent discs and the separation of the nascent disc and plasma membranes, as proposed by Steinberg et al. (1980). In this context, it is interesting that peripherin/rds has a subcellular distribution within the outer segment complementary to that of prCAD, being present along the disc rims of mature outer segments and of nascent discs on the ciliary side of the outer segment but absent from the edges of the nascent discs on the side of the outer segment opposite the connecting cilium (Arikawa et al., 1992).

We have thus far not observed evidence for homophilic binding of prCAD extracellular domains as assayed by cell aggregation in transfected mouse L cells or cell-surface binding of a fusion protein between alkaline phosphatase and the extracellular domain of prCAD (A.R. and J.N., unpublished data). These data suggest that any interactions with the extracellular domain of prCAD are likely to be heterophilic or, if homophilic, of low affinity.

Photoreceptor outer segments contain several cytoskeletal elements, including actin and tubulin filaments, that appear to function in the formation and preservation of outer segment structure. For example, dissociation of actin filaments following cytochalasin D treatment results in impaired synthesis of outer segment disks (Williams et al., 1988), suggesting involvment of the F actin localized to the base of the outer segment in the

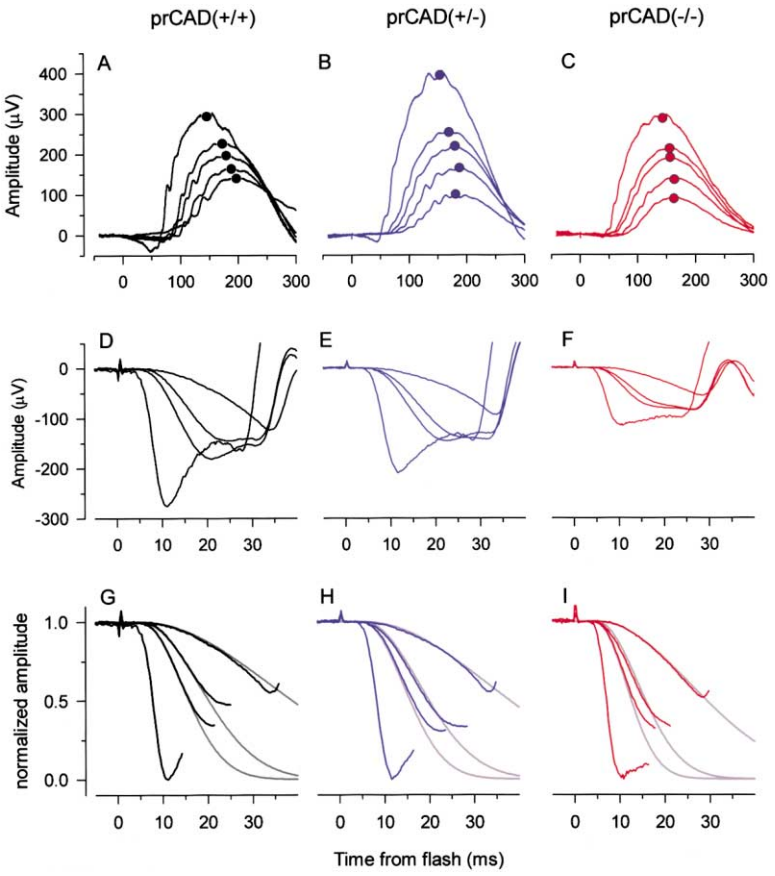

Figure 8. Functional Characteristics of *prCAD*$^{+/+}$, *prCAD*$^{+/-}$, and *prCAD*$^{-/-}$ Retinas

Each column of traces presents records from a single mouse of the genotype specified above the column.

(A–C) Scotopic b-waves of mice at 8–9 weeks of age. For each animal the traces were obtained in response to a series of 510 nm flashes whose intensities were 2.1×10^{-4}, 4.2×10^{-4}, 1.1×10^{-3}, 2.21×10^{-3}, and 1.1×10^{-2} scot. cd. s m^{-2}; we estimate that in a normal mouse, flashes of these intensities produce 0.2, 0.4, 1.0, 2.0, and 10 photoisomerizations per rod, respectively. Each trace is the average of nine individual records. The recording bandwidth was 0.1–1 KHz; sampling was 5 KHz. The peak amplitudes of the b-wave responses, filtered at 15 Hz, are superimposed on the traces (symbols).

(D–F) ERG responses from which a-waves (initial, corneal-negative components) were extracted and analyzed. Each response is the average of nine individual records from each eye (18 total traces), except for the response to the most intense flash, which is the average of two records. The flash intensities were (from least to most intense) 0.43, 2.2, 4.3, and 160 scot. cd. s m^{-2}. The saturating amplitudes of the traces are 275 μV (*prCAD*$^{+/+}$), 210 μV (*prCAD*$^{+/-}$), and 117 μV (*prCAD*$^{-/-}$).

(G–I) The traces in (D–F) are presented again, normalized by the saturating amplitudes of the a-waves, and fitted with an activation model of the phototransduction cascade (gray traces), as described in Experimental Procedures. The *prCAD*$^{+/+}$ and *prCAD*$^{-/-}$ mice were littermates.

folding of outer segment plasma membranes. As classical and desmosomal cadherins are known to recruit cytoskeletal elements to focal adhesion loci, it is possible that the cytosolic domain of prCAD functions in organizing cytoskeletal elements at the base of the outer segment. Failure of this function might account for the observed disorganization of outer segments in *prCAD*$^{-/-}$ mice many microns distal to the base of the outer segment where prCAD would normally reside. The normal localization of outer segment proteins in *prCAD*$^{-/-}$ retinas suggests that, in contrast to proteins that are localized to the connecting cilium, prCAD is not likely to participate in protein transport from the inner to the outer segment of the photoreceptor.

Photoreceptor Function in the Absence of prCAD

While the absence of prCAD severely compromises the structure of outer segments, the consequences of its absence are surprisingly mild for photoreceptor electrical signaling in young mice. Thus, our data show young

Table 1. Parameters of Electroretinograms of *prCAD* Mice

prCAD Genotype	t_{peak} (ms)	$b_{max,scot}$ (μV)	$I_{0.5}$ (scot. cd s m^{-2})	a_{max} (μV)	*KA* s^{-2}(scot. cd s m^{-2})$^{-1}$	$b_{max,pho}$ (μV)t	S_{UV}/S_M
(−/−) (n = 5)	158 ± 24	260 ± 30	(9.3 ± 4.2) × 10^{-4}	77 ± 34	4500 ± 1500	70 ± 20	1.8 ± 0.4
(+/−) (n = 3)	182 ± 11	370 ± 50	(5.8 ± 1.6) × 10^{-4}	210 ± 20	3400 ± 520	190 ± 5	1.4 ± 0.1
(+/+) (n = 5)	141 ± 41	250 ± 100	(5.9 ± 3.6) × 10^{-4}	140 ± 45	3100 ± 500	120 ± 24	1.3 ± 0.3

The first column gives the genotype of the *prCAD* mice and the number of mice tested. The first row of the remaining columns identifies a specific parameter of the ERG that was measured for each mouse, and the second row gives the physical units of the parameter. The entries in each column are the mean ± S.D. of the parameter, measured for the group of animals identified in the first column. The parameters are as follows: t_{peak} is the time to peak of the scotopic b-wave response to the two least intense flashes; $b_{max,scot}$ is the saturating amplitude; $I_{0.5}$ is the intensity that produces a half-saturating scotopic b-wave response, extracted as illustrated in Figures 8A–8C; a_{max} is the saturating amplitude of the a-wave, measured as illustrated in Figures 8D–8F; *KA* describes the efficacy of the activation steps of the rod transduction cascade (see Experimental Procedures and Figure 8G–8I); $b_{max,phot}$ is the saturating amplitude of the cone-driven b-wave, obtained in the presence of a rod-saturating steady background (see Experimental Producedures); and S_{UV}/S_M is the dimensionless ratio of the sensitivities of the cone-driven b-wave at 360 nm and 510 nm, approximately the wavelengths of the peak absorbance of the two murine cone photopigments (see Experimental Procedures; Lyubarsky et. al., 1999). ERGs were obtained from three prCAD$^{+/+}$, three prCAD$^{+/-}$, and three prCAD$^{-/-}$ mice on a 129 inbred background and from two prCAD$^{+/+}$ and two prCAD$^{-/-}$ mice on a 129/C57BL/6j mixed background. No significant ERG differences were observed between these two genetic backgrounds.

prCAD$^{-/-}$ mice to have only modest deficiencies in the amplitudes of the principal components of the ERG (Figure 8; Table 1, $b_{max,scot}$; a_{max}; $b_{max,phot}$) and in other quantitative descriptors of function ($I_{0.5}$ for the scotopic b-wave; *KA*). The most severe defect in *prCAD*$^{-/-}$ responses is in the saturated amplitude of the a-wave, which is reduced in *prCAD*$^{-/-}$ mice to 30%–50% of its amplitude in *prCAD*$^{+/+}$ or *prCAD*$^{+/-}$ mice. A defect of this magnitude would be expected if the total rod outer segment plasma membrane in the retinas of *prCAD*$^{-/-}$ mice were reduced by a similar percentage but had the normal density of cGMP-activated channels, carrying inward currents that are suppressable by the light-activated cascade.

Normal functioning of the rod transduction cascade in the absence of prCAD is also supported by the statistical equivalence of the amplification parameter, *KA,* across the three *prCAD* genotypes (Table 1). For *prCAD*$^{+/-}$ and *prCAD*$^{+/+}$ mice, this parameter can be converted into its more familiar units, s^{-2} per photoisomerization. Averaged over the eight *prCAD*$^{+/-}$ and *prCAD*$^{+/+}$ mice, the converted value is 3.4 s^{-2}, very close to that previously reported for C57BL/6j mice, 3.7 $\pm$ 0.9 s^{-2} (Lyubarsky et al., 1999). But why should *KA* be of comparable magnitude in *prCAD*$^{-/-}$ mice, which have smaller and disorganized outer segments? The likely answer is that two compensating factors cancel one another. The reduction in total rhodopsin will proportionately reduce the light collection efficiency factor *K*. This reduction, however, will be compensated by the inverse dependence of the amplification constant *A* on outer segment volume, providing that the concentrations of the transduction proteins in the smaller outer segments of the *prCAD*$^{-/-}$ mice are maintained near normal levels (Pugh and Lamb, 1993; Leskov et al., 2000). Stated alternatively, the activation phase of the rod response to a flash of a particular intensity depends ultimately on the concentration of active proteins in the outer segment, and for flashes of the intensities used here this concentration is approximately independent of the size of the outer segment.

The reduced magnitude of the saturating amplitude of the cone-driven b-wave, $b_{max,phot}$, suggests that cone function in *prCAD*$^{-/-}$ mice is compromised in a manner similar to the way rod circulating current, reflected in a_{max}, is affected. Since the cone:cone-bipolar ratio is roughly 1 in the mouse (Jeon et al., 1998; Haverkamp and Wassle, 2000), diminished cone transduction current would be expected to proportionately diminish ON-bipolar response amplitude, and thus $b_{max,phot}$. In contrast, rod:rod-bipolar convergence is probably in excess of 10:1 (Jeon et al., 1998; Haverkamp and Wassle, 2000), so that reduction in rod circulating current in *prCAD*$^{-/-}$ retinas would likely have less effect on the saturating rod-bipolar current, reflected in the parameter $b_{max,scot}$.

In summary, the electrophysiological, immunocytochemical, and ultrastructural data are consistent with the hypothesis that the absence of prCAD affects primarily the structure and size of rod and cone outer segments, while leaving the processes underlying phototransduction in rods and cones largely intact.

Involvment of prCAD in Inherited Retinal Disease

The *prCAD*$^{-/-}$ phenotype in the mouse and the high degree of conservation in prCAD sequences between mice and humans predicts that mutations in human *prCAD* are likely to cause retinal disease. At present, no retinal disease has been mapped to the human *prCAD* locus, but this may simply reflect the paucity of mapped retinal disease genes with recessive inheritance. Although the severity and time course of disease phenotype often varies in comparing the corresponding mouse and human gene mutations, genetic lesions that lead to photoreceptor degeneration in the mouse have, in general, manifest as one of several photoreceptor diseases in humans: Leber's congenital amaurosis, retinitis pigmentosa, or macular degeneration.

Experimental Procedures

cDNA and Genomic DNA Clones

Multiple independent cDNA clones encoding bovine, mouse, and chicken prCAD were isolated by DNA hybridization to oligo(dT)-primed cDNA libraries from adult bovine retina (Rattner et al., 2000), developing mouse eye (H. Sun and J.N., unpublished data), and developing chicken retina (gift of Dr. Ruben Adler). Rapid amplification of cDNA ends (RACE) was used to clone the 5′-most ~300 bp of the *cprCAD* cDNA from chicken embryonic retina RNA using the Marathon cDNA amplification kit (Clonetech). *prCAD* genomic lambda phage clones were isolated from a 129/SVJ genomic DNA library (a gift of Dr. Se-Jin Lee) using standard methods.

Sequence Analysis

Sequence alignment was performed using the Pileup and Gap programs (Genetic Computer Group, Madison, WI). The phylogenetic tree was calculated using CLUSTAL W (Thompson et al., 1994). The signal peptide and transmembrane domain were predicted using the SignalP server (www.cbs.dtu.dk/services/SignalP/; Nielsen et al., 1997) and the TMHMM server (www.cbs.dtu.dk/services/TMHMM-2.0/; Sonnhammer et al., 1998), respectively.

Chromosomal Localization

Chromosome mapping of human *prCAD* was performed using the Stanford TNG radiation hybrid panel (Research Genetics). The panel was screened by PCR with primers based on the sequence of human *prCAD* EST clone 29f4 (accession number w26443; forward primer, 5′-CTGGCCGGCACCATGGCCACCGTC; reverse primer, 5′-GGGACAGAGAGCTTTCTGGGCTGTTG). Statistical analysis using the Stanford Genome Center Radiation Hybrid server localized *prCAD* near marker SHGC-11466 on chromosome 10q22 with a LOD score of 10.17 at a distance of 22 centiRay$_{10,000}$.

RNA Blot and In Situ Hybridization

Twenty micrograms of total RNA from rat, mouse, or bovine tissues was resolved by agarose gel electrophoresis under denaturing conditions, blotted, and hybridized with mouse or bovine *prCAD* coding region probes under high stringency conditions. In situ hybridization was performed on 20 μm frozen sections of unfixed CD1 mouse retina using digoxigenin-labeled riboprobes from mouse *prCAD*, as previously described (Wilkinson 1992).

Targeted Deletion of *PrCAD*

Electroporation and culturing of ES cells (line R1), blastocyst injection, and animal breeding and genotyping were performed using standard methods. The targeted *prCAD* allele was maintained both on a mixed 129 $\times$ C57BL/6j background and on a pure 129 background.

Antibody Production and Purification

A synthetic C-terminal peptide from mouse prCAD (LKQKFEKKSLD NKAYI) was crosslinked with gluteraldehyde to BSA (Harlow and Lane, 1988) and used to immunize rabbits. Antisera were affinity-purified using the same peptide coupled to an Affi-Gel 10 matrix (Bio-Rad). A second immunogen was produced in *E. coli* as a fusion of the T7 gene 10 protein and amino acids 23–252 from mouse prCAD, purified by preparative SDS-polyacrylamide gel electrophoresis, and used for immunization of rabbits. An analogous fusion

containing the same prCAD sequences fused to maltose binding protein (MBP, New England Biolabs) was produced in *E. coli*, purified by amylose affinity chromatography, and used for affinity purification of immune sera after covalent coupling to Affi-Gel 10.

Immunohistochemistry

Mouse eyes or eyecups were fixed by immersion in 4% paraformaldehyde in PBS for 4 hr at 4°C, cryoprotected in 30% sucrose, and embedded in OCT. Frozen sections (10 μm) were incubated for 1 hr in PBS containing 10% goat serum and 0.3% Triton X-100 and incubated in PBS containing the primary antibody, 10% goat serum, and 0.3% Triton X-100 overnight at 4°C. Primary antibody was detected with fluorescein- or Texas red-conjugated goat anti-mouse or goat anti-rabbit antibodies (Vector). Anti-rhodopsin mAb 1D4 was purified using caprylic acid precipitation (Harlow and Lane, 1988) and directly conjugated to Oregon Green (Molecular Probes). Mouse anti-rhodopsin mAb 1D4, anti-ROM-1 mAb 1D5, and anti-CNCG α mAb 1D1 were gifts of Dr. Robert Molday (Molday, 1998); mouse anti-Na/K ATPase α subunit mAb α-5 was developed by Dr. Doug Fambrough and obtained from the Developmental Studies Hybridoma Bank at the University of Iowa; rabbit anti S-cone opsin antibodies are described in Wang et al. (1992); rabbit anti-arrestin antibodies were a gift of Dr. Toshi Shinohara; and rabbit anti-GFAP was from Dako. Confocal images were collected on a Zeiss LCM 510.

TUNEL Labeling

Terminal deoxynucleotide transferase-mediated dUTP nick end labeling (TUNEL) was performed on fresh-frozen retina sectioned at 14 μm, postfixed in 4% paraformaldhyde in PBS, and labeled by incorporation of fluorescein-conjugated dUTP using the in situ Cell Death Detection kit (Roche).

Plastic Sections and Electron Microscopy

Eyes were immersion-fixed in PBS containing 2% glutaraldehyde and 2% paraformaldehyde for ~20 min before removal of the lens. Eyecups were further fixed in the same fixative overnight at 4°C, then fixed in 1% osmium tetroxide, stained with 1% uranyl acetate, dehydrated, and embedded in Unicryl resin. Sections (0.5–1.0 μm) were stained with toluidine blue for light microscopy. Ultrathin sections were stained with uranyl acetate and lead citrate for transmission electron microscopy.

Immunoelectron Microscopy

Eyes were immersion-fixed in PBS containing 4% paraformaldehyde, 0.1% glutaraldehyde and 2 mM $MgCl_2$ for 10 min before dissection of the retina. Retinas were fixed for a total of 1 hr at room temperature in the same fixative and blocked with 50 mM NH_4Cl for 20 min and then with blocking solution (PBS containing 10% NGS and 0.3% Triton X-100) for 3 hr at room temperature. Retinas were incubated for 2 days at 4°C with primary antibodies in blocking solution, washed over 12 hr at room temperature with PBS containing 0.3% Triton X-100, incubated overnight with 0.8 nm gold-conjugated goat anti-rabbit antibodies (Aurion, The Netherlands) at a 1:10 dilution in blocking solution at 4°C, and washed overnight at 4°C. The low level of background immunogold labeling within both the inner and outer segments and the dependence of this background on the primary antibody suggests that the primary and secondary antibodies have access to both the inner and outer segments. Retinas were fixed in 2% paraformaldehyde and 2% glutaraldhyde in PBS overnight before silver enhancement and embedding in Epon resin for transmission electron microscopy.

Electroretinography

Electrical Recordings

The methods of ERG recording have been described in detail previously (Lyubarsky et al., 1999). In brief, ERGs were recorded from anesthetized mice with a differential amplifier with bandwidth 0.1 Hz to 1 KHz and were sampled and digitized at 5 KHz. The corneal electrode was a platinum wire, while the reference electrode was a tungsten needle inserted subcutaneously in the forehead. The recording chamber served dually as a Faraday cage and a ganzfeld, with ports and baffles for illumination. Mice for ERG testing were housed in dim light from birth to minimize any effects of chronic light exposure on retinal function. Mice were tested at 8–9 weeks of age. They were dark-adapted over night and prepared for recording under dim red light. Before recording commenced, animals were maintained in complete darkness for 15 min.

Light Calibrations

The methods used for light stimulation and calibration of light stimuli have been given in detail in Lyubarsky et al. (1999). Flash and steady light intensities were calibrated in terms of photons μm^{-2} or photons $\mu m^{-2}\ s^{-1}$ at the cornea; these numbers represent the flux density incident upon a photodiode positioned at the location of the mouse's eye in the ganzfeld stimulator. In previous reports, stimulus intensities were then converted into estimated numbers (or rates) of photoisomerizations, obtained by dividing the photon flux density at the cornea by the surface area of the retina, and multiplying by the estimated end-on collecting area of a rod or cone. Because the rod and cone outer segments of *prCAD*$^{-/-}$ mice are highly disorganized, conversion of intensities to photoisomerizations is problematic, and so we report flash illumination for experiments involving rod-driven ERG components in standard photometric units, scotopic candela $s\ m^{-2}$ (scot. Cd. $s\ m^{-2}$) (cf. Wyszecki and Stiles, 1982). We have determined the area of the dilated pupil of young C57BL/6j mice to be ≈3 mm^2 (Pennesi et al., 1998). Assuming this pupil area for the mice investigated here, we estimate a ganzfeld having the luminance 1 scot. cd. m^{-2} will produce 940 photoisomerizations $rod^{-1}\ s^{-1}$ (cf. Pennesi et al., 1998).

Analysis of Rod A-Waves

The a-wave of the ERG is the field potential generated primarily by massed suppression of the circulating current of rods. We analyzed a-waves with a model of the activation phase of the rod transduction cascade (Lamb and Pugh, 1992). The model predicts a-waves to obey the relation

$$1 - \frac{a(t)}{a_{max}} = \exp[-\tfrac{1}{2}\phi\, A(t - t_{eff})^2] \quad (1)$$

where $a(t)$ is the a-wave, a_{max} is its saturating amplitude, ϕ is the number of photoisomerizations rod^{-1} produced by a particular flash, A is a parameter (the amplification constant) characterizing the composite gain of the cascade steps, and t_{eff} is a brief delay. This model was fitted to an ensemble of a-wave responses of each mouse and modified to incorporate a mammalian rod membrane time constant of 1 ms (Smith and Lamb, 1997). The conversion of flash intensity expressed in luminance units to photoisomerizations rod^{-1} can be written $\phi = KI$, where I is the time-integrated luminance of the ganzfeld wall, and K is a constant that incorporates a number of eye-specific factors (see e.g., Lyubarsky and Pugh, 1996; Lyubarsky et al., 1999). Because of the defects in photoreceptor structure in *prCAD*$^{-/-}$ mice, K cannot be estimated unequivocally for these animals, and so we report the results of applying equation 1 in terms of the product, KA, which has the units $(scot.\ Cd.\ s\ m^{-2})^{-1}\ s^{-2}$.

Acknowledgments

The authors thank the members of the Johns Hopkins Transgenic Core Facility for blastocyst injection, the Howard Hughes Medical Institute Biopolymers Core Facility for DNA sequencing, and Tudor Badea and King-Wai Yau for helpful comments on the manuscript. This work was supported by the Howard Hughes Medical Institute (P.M.S., J.W., and J.N.), the National Eye Institute (A.R., J.N., A.L., A.S., and E.N.P.), and Research to Prevent Blindness (E.N.P.).

Received August 13, 2001; revised October 3, 2001.

References

Angst, B.D., Marcozzi, C., and Magee, A.I. (2001). The cadherin superfamily. J. Cell Sci. *114*, 629–641.

Arikawa, K., Molday, L.L., Molday, R.S., and Williams, D.S. (1992). Localization of peripherin/rds in the disk membranes of cone and rod photoreceptors: relationship to disk membrane morphogenesis and retinal degeneration. J. Cell Biol. *116*, 659–667.

Beech, P.L., Pagh-Roehl, K., Noda, Y., Hirokawa, N., Burnside, B., and Rosenbaum, J.L. (1996). Localization of kinesin superfamily

proteins to the connecting cilium of fish photoreceptors. J. Cell Sci. *109*, 889–897.

Cepek, K.L., Shaw, S.K., Parker, C.M., Russell, G.J., Morrow, J.S., Rimm, D.L., and Brenner, M.B. (1994). Adhesion between epithelial cells and T lymphocytes mediated by E-cadherin and the alpha E beta 7 integrin. Nature *372*, 190–193.

Chang, G.Q., Hao, Y., and Wong, F. (1993). Apoptosis: final common pathway of photoreceptor death in rd, rds, and rhodopsin mutant mice. Neuron *11*, 595–605.

Clarke, G., Goldberg, A.F., Vidgen, D., Collins, L., Ploder, L., Schwarz, L., Molday, L.L., Rossant, J., Szel, A., Molday, R.S., et al. (2000). Rom-1 is required for rod photoreceptor viability and the regulation of disk morphogenesis. Nat. Genet. *25*, 67–73.

de Raad, S., Szczesny, P.J., Munz, K., and Reme, C.E. (1996). Light damage in the rat retina: glial fibrillary acidic protein accumulates in Muller cells in correlation with photoreceptor damage. Ophthalmic Res. *28*, 99–107.

Goodyear, R., and Richardson, G. (1999). The ankle-link antigen: an epitope sensitive to calcium chelation associated with the hair-cell surface and the calycal processes of photoreceptors. J. Neurosci. *19*, 3761–3772.

Hagstrom, S.A., Duyao, M., North, M.A., and Li, T. (1999). Retinal degeneration in tulp1-/- mice: vesicular accumulation in the interphotoreceptor matrix. Invest. Ophthalmol. Vis. Sci. *40*, 2795–2802.

Harlow, E., and Lane, D. (1988). Antibodies; a Practical Approach. (Cold Spring Harbor, N.Y.: Cold Spring Harbor Laboratory Press.).

Haverkamp, S., and Wassle, H. (2000). Immunocytochemical analysis of the mouse retina. J. Comp. Neurol. *424*, 1–23.

Hong, D.H., Pawlyk, B.S., Shang, J., Sandberg, M.A., Berson, E.L., and Li, T. (2000). A retinitis pigmentosa GTPase regulator (RPGR)-deficient mouse model for X-linked retinitis pigmentosa (RP3). Proc. Natl. Acad. Sci. USA *97*, 3649–3654.

Hong, D.H., Yue, G., Adamian, M., and Li, T. (2001). Retinitis pigmentosa GTPase regulator (RPGR)-interacting protein is stably associated with the photoreceptor ciliary axoneme and anchors RPGR to the connecting cilium. J. Biol. Chem. *276*, 12091–12099.

Honjo, M., Tanihara, H., Suzuki, S., Tanaka, T., Honda, Y., and Takeichi, M. (2000). Differential expression of cadherin adhesion receptors in neural retina of the postnatal mouse. Invest. Ophthalmol. Vis. Sci. *41*, 546–551.

Jeon, C.J., Strettoi, E., and Masland, R.H. (1998). The major cell populations of the mouse retina. J. Neurosci. *18*, 8936–8946.

Kohmura, N., Senzaki, K., Hamada, S., Kai, N., Yasuda, R., Watanabe, M., Ishii, H., Yasuda, M., Mishina, M., and Yagi, T. (1998). Diversity revealed by a novel family of cadherins expressed in neurons at a synaptic complex. Neuron *20*, 1137–1151.

Lamb, T.D., and Pugh, E.N., Jr. (1992). A quantitative account of the activation steps involved in phototransduction in amphibian photoreceptors. J. Physiol. *449*, 719–758.

Leskov, I.B., Klenchin, V.A., Handy, J.W., Whitlock, G.G., Govardovskii, V.I., Bownds, M.D., Lamb, T.D., Pugh, E.N., Jr., and Arshavsky, V.Y. (2000). The gain of rod phototransduction: reconciliation of biochemical and electrophysiological measurements. Neuron *27*, 525–537.

Li, T., Snyder, W.K., Olsson, J.E., and Dryja, T.P. (1996). Transgenic mice carrying the dominant rhodopsin mutation P347S: evidence for defective vectorial transport of rhodopsin to the outer segments. Proc. Natl. Acad. Sci. USA *93*, 14176–14181.

Liu, X., Vansant, G., Udovichenko, I.P., Wolfrum, U., and Williams, D.S. (1997). Myosin VIIa, the product of the Usher 1B syndrome gene, is concentrated in the connecting cilia of photoreceptor cells. Cell Motil. Cytoskeleton *37*, 240–252.

Liu, X., Udovichenko, I.P., Brown, S.D., Steel, K.P., and Williams, D.S. (1999). Myosin VIIa participates in opsin transport through the photoreceptor cilium. J. Neurosci. *19*, 6267–6274.

Lolley, R.N., Rong, H., and Craft, C.M. (1994). Linkage of photoreceptor degeneration by apoptosis with inherited defect in phototransduction. Inv. Ophthalmol. Vis. Sci. *35* 358–3.62.

Lyubarsky, A.L., and Pugh, E.N., Jr. (1996). Recovery phase of the murine rod photoresponse reconstructed from electroretinographic recordings. J. Neurosci. *16*, 563–571.

Lyubarsky, A.L., Falsini, B., Pennesi, M.E., Valentini, P., and Pugh, E.N., Jr. (1999). UV- and midwave-sensitive cone-driven retinal responses of the mouse: a possible phenotype for coexpression of cone photopigments. J. Neurosci. *19*, 442–455.

Marszalek, J.R., Liu, X., Roberts, E.A., Chui, D., Marth, J.D., Williams, D.S., and Goldstein, L.S. (2000). Genetic evidence for selective transport of opsin and arrestin by kinesin-II in mammalian photoreceptors. Cell *102*, 175–187.

Molday, R.S. (1998). Photoreceptor membrane proteins, phototransduction, and retinal degenerative diseases. Invest. Ophthalmol. Vis. Sci. *39*, 2491–2513.

Muresan, V., Joshi, H.C., and Besharse, J.C. (1993). Gamma-tubulin in differentiated cell types: localization in the vicinity of basal bodies in retinal photoreceptors and ciliated epithelia. J. Cell Sci. *104*, 1229–1237.

Muresan, V., Bendala-Tufanisco, E., Hollander, B.A., and Besharse, J.C. (1997). Evidence for kinesin-related proteins associated with the axoneme of retinal photoreceptors. Exp. Eye Res. *64*, 895–903.

Nielsen, H., Engelbrecht, J., Brunak, S., and Heijne, G. (1997). Identification of prokaryotic and eukaryotic signal peptides and prediction of their cleavage sites. Protein Eng. *10*, 1–6.

Nollet, F., Kools, P., and van Roy, F. (2000). Phylogenetic analysis of the cadherin superfamily allows identification of six major subfamiles besides several solitary members. J. Mol. Biol. *299*, 551–572.

Pennesi, M.E., Lyubarsky, A.L., and Pugh, E.N., Jr. (1998). Extreme responsiveness of the pupil of the dark-adapted mouse to steady retinal illumination. Invest. Ophthal. Vis. Sci. *39*, 2148–2156.

Portera-Cailliau, C., Sung, C.-H., Nathans, J., and Adler, R. (1994). Apoptotic photoreceptor cell death in mouse models of retinitis pigmentosa. Proc. Natl. Acad. Sci. USA *91*, 974–978.

Pugh, E.N., Jr., and Lamb, T.D. (1993). Amplification and kinetics of the activation steps in phototransduction. Biochim. Biophys. Acta *1141*, 111–149.

Pugh, E.N., Jr., Falsini, B., and Lyubarsky, A.L. (1998). The origin of the major rod- and cone-driven components of the rodent electroretinogram and the effect of age and light-rearing history on the magnitude of these components. In Photostasis and Related Phenomena, T. Williams and A. Thistle, eds. (New York: Plenum Press), pp. 93–128.

Rattner, A., Smallwood, P.M., and Nathans, J. (2000). Identification and characterization of all-trans-retinol dehydrogenase from photoreceptor outer segments, the visual cycle enzyme that reduces all-trans-retinal to all-trans-retinol. J. Biol. Chem. *275*, 11034–11043.

Sanyal, S., De Ruiter, A., and Hawkins, R.K. (1980). Development and degeneration of retina in rds mutant mice: light microscopy. J. Comp. Neurol. *194*, 193–207.

Semple-Rowland, S.L. (1991). Expression of glial fibrillary acidic protein by Muller cells in rd chick retina. J. Comp. Neurol. *305*, 582–590.

Senzaki, K., Ogawa, M., and Yagi, T. (1999). Proteins of the CNR family are multiple receptors for Reelin. Cell *110*, 635–647.

Smith, N.P., and Lamb, T.D. (1997). The a-wave of the human electroretinogram recorded with a minimally invasive technique. Vis. Res. *37*, 2943–2952.

Sonnhammer, E.L.L., von Heijne, G., and Krogh, A. (1998). A hidden Markov model for predicting transmembrane helices in protein sequences. In Proceedings of Sixth International Conference on Intelligent Systems for Molecular Biology, J. Glasgow, T. Littlejohn, F. Major, R. Lathrop, D. Sankoff, and C. Sensen, eds. (Menlo Park, CA: AAAI Press), pp. 175–182.

Steinberg, R.H., Fisher, S.K., and Anderson, D.H. (1980). Disc morphogenesis in vertebrate photoreceptors. J. Comp. Neurol. *190*, 501–518.

Sung, C.-H., Makino, C., Baylor, D., and Nathans, J. (1994). A rhodopsin gene mutation responsible for autosomal dominant retinitis pigmentosa results in a protein that is defective in localization to the photoreceptor outer segment. J. Neurosci. *14*, 5818–5833.

Tepass, U., Truong, K., Godt, D., Ikura, M., and Peifer, M. (2000). Cadherins in embryonic and neural morphogenesis. Nature Rev. Mol. Cell. Biol. *1*, 91–100.

Thompson, J.D., Higgins, D.G., and Gibson, T.J. (1994). CLUSTAL W: improving the sensitivity of progressive multiple sequence alignment through sequence weighting, positions-specific gap penalties and weight matrix choice. Nucleic Acids Res. *22*, 4673–4680.

Travis, G.H., Groshan, K.R., Lloyd, M., and Bok, D. (1992). Complete rescue of photoreceptor dysplasia and degeneration in transgenic retinal degeneration slow (rds) mice. Neuron *9*, 113–119.

Wang, Y., Macke, J.P., Merbs, S.L., Zack, D.J., Klaunberg, B., Bennett, J., Gearhart, J., and Nathans, J. (1992). A locus control region adjacent to the human red and green visual pigment genes. Neuron *9*, 429–440.

Whitehead, J.L., Wang, S.Y., Bost-Usinger, L., Hoang, E., Frazer, K.A., and Burnside, B. (1999). Photoreceptor localization of the KIF3A and KIF3B subunits of the heterotrimeric microtubule motor kinesin II in vertebrate retina. Exp. Eye Res. *69*, 491–503.

Wilkinson, D.G. (1992). In Situ Hybridization: a Practical Approach. (Oxford: IRL Press).

Williams, D.S., Linberg, K.A., Vaughan, D.K., Fariss, R.N., and Fisher, S.K. (1988). Disruption of microfilament organization and deregulation of disk membrane morphogenesis by cytochalasin D in rod and cone photoreceptors. J. Comp. Neurol. *272*, 161–176.

Wohrn, J.C., Puelles, L., Nakagawa, S., Takeichi, M., and Redies, C. (1998). Cadherin expression in the retina and retinofugal pathways of the chicken embryo. J. Comp. Neurol. *396*, 20–38.

Wyszecki, G., and Stiles, W.S. (1982). Color Science, second ed. (New York: John Wiley & Sons).

Yagi, T., and Takeichi, M. (2000). Cadherin superfamily genes: functions, genomic organization, and neurologic diversity. Genes Dev. *14*, 1169–1180.

Young, R.W. (1971). The renewal of rod and cone outer segments in the rhesus monkey. J. Cell Biol. *49*, 303–318.

Accession Numbers

Human, mouse, chicken, rat, and bovine prCAD sequences can be found in GenBank under accession numbers AB053448, AF426393, AF426394, AB053449, and AF426392, respectively. (New accession numbers are for mouse, chicken, and bovine; human and rat had previously been deposited.)